Simulation of the Effects of Force and Heat Produced by a Plasma Actuator on Neutral Flow Evolution

G. I. Font[*], S. Jung[†], C. L. Enloe[‡], T.E. McLaughlin[§]
United States Air Force Academy

W. L. Morgan[**]
Kinema Research, L.L.C.

J. W. Baughn[††]
University of California, Davis

Particle and fluid simulations are carried out of a plasma actuator discharge. Particle-in-Cell Direct-Simulation-Monte-Carlo (PIC-DSMC) simulations of a pure oxygen discharge are conducted to characterize the force and heating characteristics a typical discharge. The results show that the plasma imparts a force which points upstream during the first half of the bias cycle and points downstream during the second half of the cycle. The upstream force, however, is as much as 20 times smaller than the downstream force. The results from the particle simulations are, then, inserted into a Navier-Stokes fluid code to explore the effects on the neutral flow. Fluid simulations confirm that the force produced in the particle simulations create a flow similar to a wall jet in the vicinity of the plasma actuator. The results of heat addition show that it can not account for the force levels observed in experiments, but can account for density reductions.

I. Introduction

Plasma actuators have demonstrated the ability to promote boundary layer attachment on airfoils at a high angle-of-attack. This technology holds the promise of increasing the lift and/or reducing the drag of airfoils and fuselages through electronic means, where as previously only pneumatic or physical options were available.[1-5] Experiments and simulations have shown that the boundary layer attachment promotion

takes place because the plasma actuator imparts momentum to the flow.[4-6] The plasma actuator is a rather simple device. Figure 1 illustrates its components. Two electrodes are separated by a dielectric and staggered in the flow direction. The electrodes are subjected to an alternating bias of several thousand volts at a frequency in the kilohertz to tens of kilohertz range. This results in a dielectric barrier discharge from the exposed to the buried electrode and a force which accelerates the flow downstream.
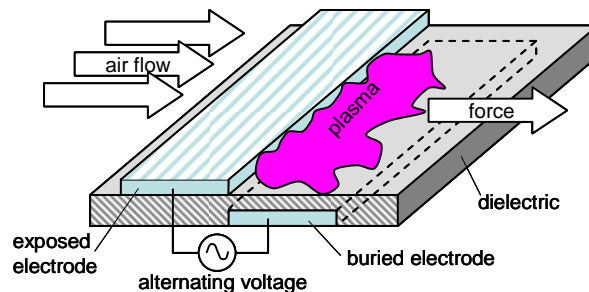

Figure 1. Plasma actuator configuration.

[*] Associate Professor, Department of Physics, USAF Academy, CO 80840, Member, AIAA.
[†] Visiting Scientist, Department of Aeronautics, USAF Academy, CO 80840.
[‡] Professor, Department of Physics, USAF Academy, CO 80840, Senior Member, AIAA.
[§] Director, Aeronautics Research Center, Department of Aeronautics, USAF Academy, CO 80840, Associate Fellow, AIAA.
[**] Chief Scientist, Kinema Research, L.L.C., Monument, CO, 80132
[††] Professor, Department of Mechanical and Aeronautical Engineering, University of California, Davis, Davis, CA 95616, Member, AIAA.

In previous numerical studies,[7,8] we explored the force production mechanism of the plasma in Nitrogen and Oxygen. Simulations showed that the plasma is pulling on the air during the first half of the bias cycle and pushing during the second half. A net force arises because the plasma density and, therefore, momentum transfer are greater during the second half of the bias cycle. Further numerical studies using Oxygen showed that the presence of negative ions in the air do not change the force production characteristics. The level of negative oxygen ions generated by the plasma in the air are not sufficient to reverse the direction of the force imparted to the air, although, they do have a significant effect on the efficiency of the actuator.

The numerical code used in these studies was based on particle methods (PIC-DSMC) and followed positive and negative ions, electrons, and their interactions with the air. However, it did not attempt to model the response of the air after the momentum transfer from the charged species. This did not compromise the results of the simulations since the discharge time scale is on the order of nanoseconds while the air response time scale is on the order of milliseconds. In the present work, the results of the particle code are supplied as source terms to a Navier-Stokes fluid code to check for consistency with observed experimental results. Section II will summarize the force production characteristics as derived from the particle methods studies. The third section will detail the neutral fluid response to the plasma generated force as calculated by a neutral fluid code. Part IV will examine the heat deposition characteristics as calculated by the particle code. The fifth part will use the particle derived heat deposition and the fluid code to explore the effects on the neutral flow. The final part will summarize the findings.

II. Force Production Derived from Particle Computations

The plasma discharge was computed utilizing a Particle-in-Cell Direct-Simulation-Monte-Carlo (PIC-DSMC) technique.[9-13] Electrons, positive ions, and negative ions are tracked through a computational mesh. Their positions are used to calculate a charge distribution on the mesh which is, in turn, used to compute the potential distribution through a solution of the Poisson's equation. The resulting distribution is differentiated for the electric field which gives the force on the charged particles. A leap-frog scheme[9] is, then, used to update the velocities and positions of all particles. Collisions with neutrals are handled through a DSMC technique.[10,11] The probability of collision is calculated from the collision cross sections[14-18] and a random number generator is used to determine which collisions take place. Neutral particles involved in collisions are generated from Maxwellian distributions for each event. After the collisions, the neutral particles are discarded and are not tracked further. This reduces the computational load to a tractable level since neutral movement and neutral-neutral collisions do not have to be computed. The computational grid is displayed in Fig. 2. The edge of the exposed electrode, the dielectric, and the buried electrode are included in the computation. Previous experimental and computational studies[7,8,19,20] have shown that the plasma does not extend upstream of the edge of the exposed electrode, therefore,
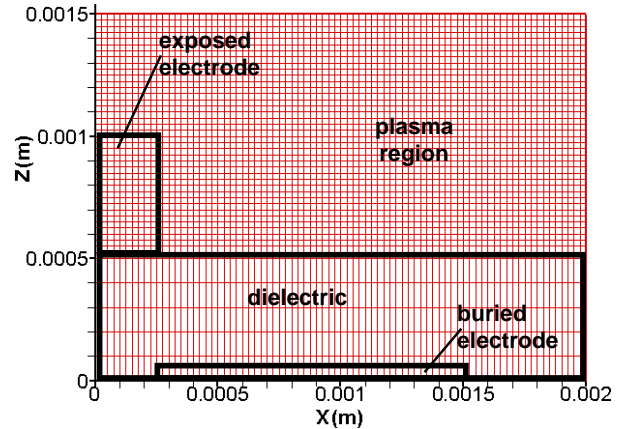

Figure 2. Computational geometry.

Table 1. Oxygen Chemical Reactions

e	+ O_2	$\rightarrow$	O_2	+	e	momentum transfer
e	+ $2O_2$	$\rightarrow$	O_4^+	+	2e	ionization ($O_2 + O_2^+ \rightarrow O_4^+$)
e	+ O_2	$\rightarrow$	O-	+	O	dissociative attachment
e	+ O_2	$\rightarrow$	O_2^*	+	e	meta-stable excitation
e	+ O_2	$\rightarrow$	2O	+	e	dissociation
e	+ O_4^+	$\rightarrow$	$2O_2$			dissociative recombination (glow)
O_4^+	+ O_2	$\rightarrow$	O_4^+	+	O_2	momentum transfer
O-	+ O_2	$\rightarrow$	O-	+	O_2	momentum transfer
O-	+ O_4^+	$\rightarrow$	$2O_2$	+	O	recombination
O_4^+	+ Cu_{surf}	$\rightarrow$	$2O_2$	+	0.03e	secondary electron emission

2
American Institute for Aeronautics and Astronautics

truncating the computation at the electrode edge is justified. The computational domain is 2.0 x 1.5 x 0.1mm. Although the particle motion is resolved in 3D, the small width of the domain effectively makes this a 2D approximation of the discharge. Only a subset of the cells are shown for clarity. The smallest cells have sides on the order of a micron.

Computations have been carried out in pure oxygen and pure nitrogen separately. Pure nitrogen is used to explore electropositive gasses and pure oxygen is used to represent electronegative gasses. Because oxygen dissociates and ionizes at lower energies than nitrogen, the oxygen dominates the discharge chemistry in air. Computations in pure oxygen are, therefore, more representative of the chemistry in air and will be used in the present study. The reactions used in oxygen calculations are shown in Table I. They include dissociation, meta-stable excitation, ionization, dissociative attachment, dissociative recombination, ion-ion recombination, elastic collisions, and secondary electron emission at the walls.

The force vectors from a typical computation are shown in Fig. 3. The figure displays the region in the vicinity of the exposed electrode edge and the surface of the dielectric. The voltage was set to 4500 volts (0-peak). The vectors of the first half of the bias cycle are increased in size for clarity. During the first half of the bias cycle, the forward discharge, the force is predominantly upstream. During the latter half of the bias cycle, the back discharge, the force is predominantly downstream. This occurs because the ion elastic collision cross-sections at the present ion energies are more than an order of magnitude larger than the electron elastic collision cross-sections.[8] The result is that the ions dominate the momentum transfer to the neutrals. Since they are pulled by the electric field during the first half of the cycle, the force to the air is initially upstream. When the field reverses, during the second half of the bias cycle, the ion dominated force points downstream. If the force vectors are added together, the total downstream average force is a factor of about 20 larger than the total upstream force. The net results on the air is, therefore, a force which is on the average, pointed downstream. The force imbalance occurs because the ion density is a factor of 10, or more, greater during the second half of the cycle. The ion density is not equal during both halves of the bias cycle because the first half of the discharge begins from a few cosmic or field-effect emitted electrons, while the second half of the discharge begins from all of the electrons deposited on the dielectric during the first half of the bias cycle.
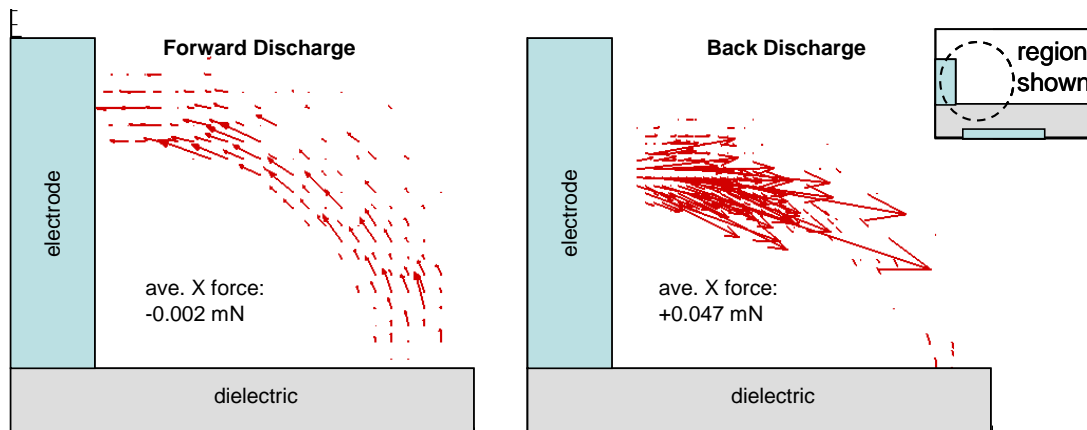

Figure 3. Force vectors and average force during forward and back plasma discharge for a single streamer in Oxygen; peak bias = 4500 V. The vectors for the forward discharge are exaggerated for clarity.

III. Force Production Applied to Fluid Computations

In order to test whether, the force characteristics (initially pointed upstream and later pointed downstream) are compatible with the experimentally observed behavior of the air, the results of the PIC-DSMC computations were inserted into a Navier-Stokes fluid code using momentum source terms. The code utilized was the commercially available and exhaustively documented FLUENT. The grid, illustrated in Fig. 4, is 40cm long and 20cm high and 2 dimensional. The figure shows the region near the edge of the exposed electrode. A time varying momentum source term was applied to still air with a frequency of 5000Hz. The force was applied initially upstream and later downstream as indicated by the particle simulations. The peak magnitude of the downstream force was set to be a factor of 20 larger than the upstream force.
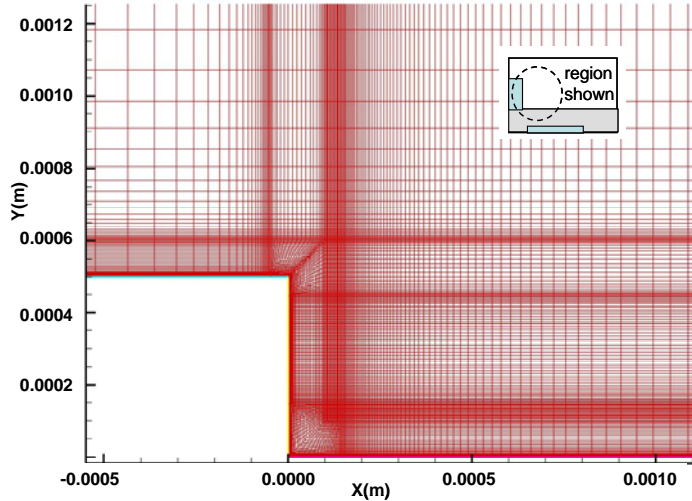

Figure 4. Navier-Stokes code grid near the edge of the exposed electrode.

The force-time relation was constructed by noting when the plasma was observed to exist in the experiments. Figure 5a shows the current measurements from experiments and applied voltage[20]. The plasma exists, to first order, during the first quarter cycle (forward discharge) and during the third quarter cycle (backward discharge). The plasma density grows exponentially during each discharge, as suggested by the particle simulations. Since the force on the ions is a function of the plasma density, the force should also initially grow exponentially. When the voltage, however, is insufficient to continue the discharge, the plasma density and force should decrease as ions are destroyed through recombination at the walls or in the field. In order to investigate the effect on the air in the simplest manner, a half of a sine function was chosen to represent the plasma density –and corresponding force, for each discharge, as shown in Fig. 5b. The initial discharge produces a negative (upstream) force. The second discharge produces a positive (downstream) force. The relative size of the forces was taken from the particle simulations to be a factor of about 20. The total integrated force was scaled to produce an average force of about 1.5mN, which is representative of the experiments.
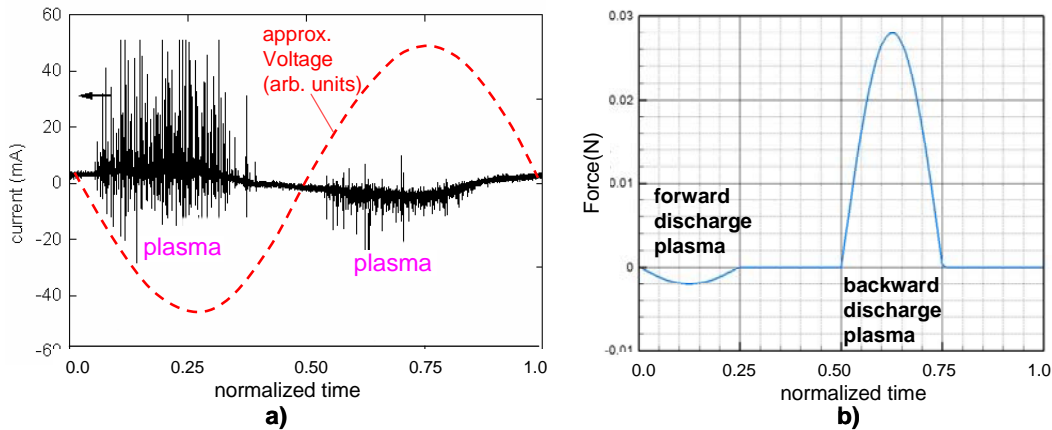

Figure 5. a) Experimental current measurements. b) Temporal force schedule used in Navier-Stokes computation to align force production with plasma during one bias cycle.

4

The force schedule was applied as a momentum source term to air which was initially not moving. The force was applied over a region that was 0.5mm high by 5mm long. This represents the maximum region where the plasma is observed to exist. The maximum height of the plasma is typically about the size of the thickness of the exposed electrode and the length of the plasma is never longer than the length of the buried electrode. A 2nd order time-accurate Newtonian sub-iteration scheme was applied to evolve the flow and follow the unsteady fluctuations. Two-hundred time steps were converged during each bias cycle.
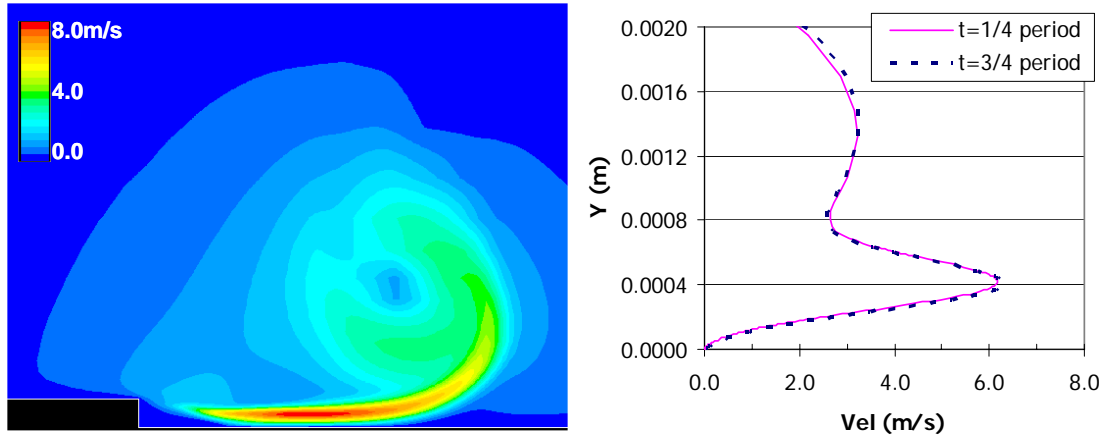

Figure 6. **Velocity magnitude contours and x velocity profile 0.08 sec. after plasma actuator initiation. Velocity profile is from a position 0.005m downstream of the exposed electrode step and at times ¼ and ¾ through the bias period.**

The results of inserting the particle code force results into the fluid code are shown in Fig. 6, which displays the velocity magnitude contours and x velocity profile at a time 0.08 seconds after the plasma actuator was started. The plasma actuator creates a flow similar to a wall jet, imparting momentum to the flow over a very small region. At this time in the computation, the starting vortex has not yet moved a significant distance from the exposed electrode. As more flow is entrained, this vortex will move downstream. The x velocity profile, taken at a point 0.005m downstream of the exposed electrode edge, is also shown in Fig. 6. The maximum velocity is about 6 m/s and is located at less than one millimeter from the wall. The second velocity peak, located at 1.4mm from the wall is simply part of the starting vortex and will vanish as the vortex moves away. Similar wall jets have been observed experimentally[21], although, direct comparison is not possible since measurements were not taken this close to the actuator and at such a short time period after plasma start. It is interesting to note that the velocity distributions at the ¼ and ¾ time in the period are so similar. The ¼ time is when the plasma ends pulling the flow upstream. This is where we would expect to find negative or slowest velocity. The ¾ time is when the plasma has completed its downstream push and where the largest velocities would be expected. While this is, in fact, what is found in the computations, the difference between the largest and smallest velocities is less than 2%. Negative flow is generated, but only within a space less than 1mm from the edge of the exposed electrode. This is, perhaps, not unexpected since the total force generated by the actuator pulling upstream is only $1/20^{th}$ of that which is generated pushing downstream.

IV. Heat Addition Derived from Particle Computations and Experiments

The plasma discharge created by the actuator affects the neutral flow through several important mechanisms: 1) momentum addition, 2) heat addition, and 3) composition alteration (dissociation and other chemical reactions). In this section, the second of these effects, heat addition, will be characterized.

American Institute for Aeronautics and Astronautics

Figure 7 displays the temporal light measurements as a function of time, applied voltage, and distance away from the exposed electrode[22]. The plasma is created and destroyed twice during a bias cycle, as already noted in Fig. 5. During each plasma creation phase, the discharge begins at the edge of the exposed electrode and marches downstream. Very little plasma is seen upstream of the exposed electrode.
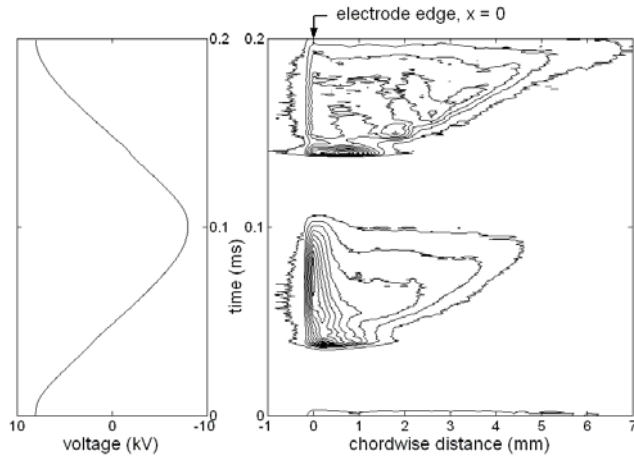
Particle simulations of multiple discharges give a clue as to how the plasma may be expanding. Discharges were simulated in pure nitrogen for a bias voltage amplitude of 5000 V. The initial plasma discharge was allowed to reach the dielectric surface before a second discharge was initiated by reseeding the flow field near the exposed electrode with the same small seed number of electrons which began the first discharge. Figure 8 shows the resulting charge density contours. The initial discharge creates a plasma which reaches about 1mm away from the exposed electrode. The charged particles from the first discharge begin to shield out the electric field which pulls the electron trajectories toward the buried electrode. This causes the electron trajectories of the second discharge to be more horizontal, resulting in the second discharge traveling about 20% farther than the first discharge. In a plasma with repeated streamer discharges, therefore, the plasma region would begin near the exposed electrode and subsequently move away along the extent of the buried electrode, as each follow-on streamer reached further away from the exposed electrode. The region of ionization, dissociation, excitation, and their associated heating of the neutrals, therefore, also moves away from the exposed electrode. This is precisely what is observed in experiments: a plasma that begins near the exposed electrode and then expands downstream. This plasma expansion occurs twice during a plasma bias cycle: once, during all of the plasma streamers that make up the forward discharge, and a second time, during all of the plasma streamers that make up the back discharge.

Figure 7. Plasma light emission measurements as a function of time, bias voltage, and distance away from the edge of the exposed electrode.
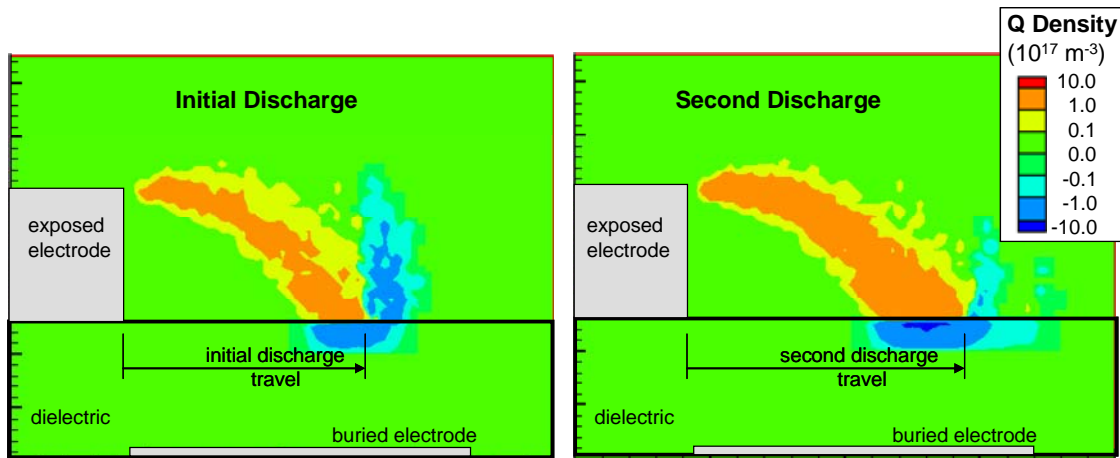
Figure 8. Particle simulation charge density contours after initial and a follow-on plasma discharge. Discharge simulated in pure nitrogen for a bias amplitude of 5000V.

The bulk of the neutral heating is done by the electrons through inelastic processes: ionization, dissociation, and excitation. Since the electrons sufficiently energetic to suffer inelastic collisions are found at the head of the streamer (the blue regions outside the dielectric in Fig. 8), the region where the neutrals are being heated may predominantly be a small area near the head of the streamer. This small area

American Institute for Aeronautics and Astronautics

starts near the exposed electrode and moves away, sweeping the total extent of the plasma twice during a bias cycle. An approximation of this moving heating region will be used in the fluid simulations of the neutral flow.

V. Heat Addition Applied to Fluid Computations

In order to simulate the heating effects of the plasma on the neutrals, the fluid computations will utilize a moving heating zone, as suggested by the particle simulations and the experiments. A typical plasma actuator is operated at a power level of tens of Watts. It is difficult to determine how much of this power goes into directly heating the flow versus how much goes into ionization, dissociation, excitation, and other chemical processes. The previous sections of this work assumed a total power level of about 20W. For this section, it will be assumed that half of the total energy goes directly into heating the neutral flow. This is meant as an approximation only and can be refined in future simulations. The heating zone is set to the rough dimensions of the energetic electron head of the plasma streamer: 0.2mm wide (from the particle simulations) and 0.5 mm high (the maximum height of the plasma). The heating zone will start at the edge of the exposed electrode and travel downstream along the length of the plasma, a distance assumed to be roughly 5mm. The total heat addition in the zone is adjusted to be equivalent to 10W over an actuator which is 250mm wide or 40W per meter for the 2D simulation.
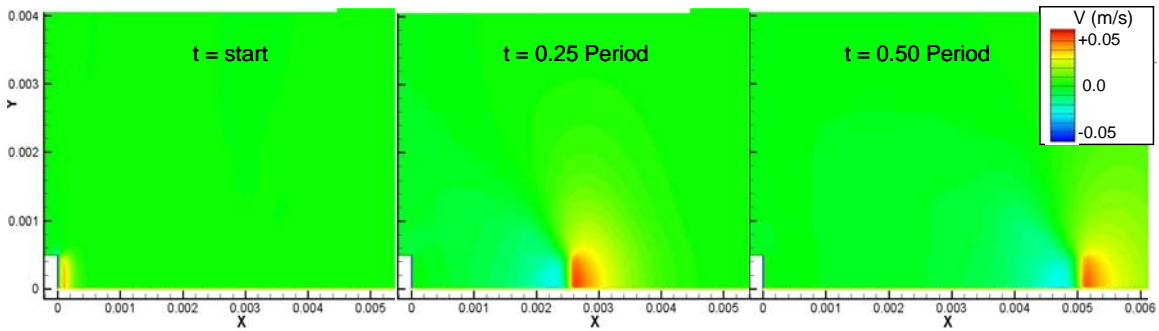

Figure 9. Velocity distribution during forward plasma discharge heat addition (1/2 bias cycle). Total heat addition is 10W at 5000Hz.

The velocity distribution contours through the forward half of the discharge are shown in Fig. 9. The added heat causes the flow to expand against the exposed electrode edge and begin to move downstream. As the heating zone travels downstream, the air on the right of the heating zone is always accelerated by the expanding gas, while the air on the left it is decelerated. The maximum local velocity achieved is 0.05m/s. The computations where the plasma force was directly applied to the flow (section III) resulted in velocities in excess of 5m/s over the same region. Therefore, plasma heat addition does not appear to play a significant part in accelerating the neutrals.

Figure 10 displays the temperature and density distribution after hundreds of bias cycles as computed by the fluid code. The effect of 10W of heat addition is to raise local the temperature 17 degrees Kelvin. Experimental studies
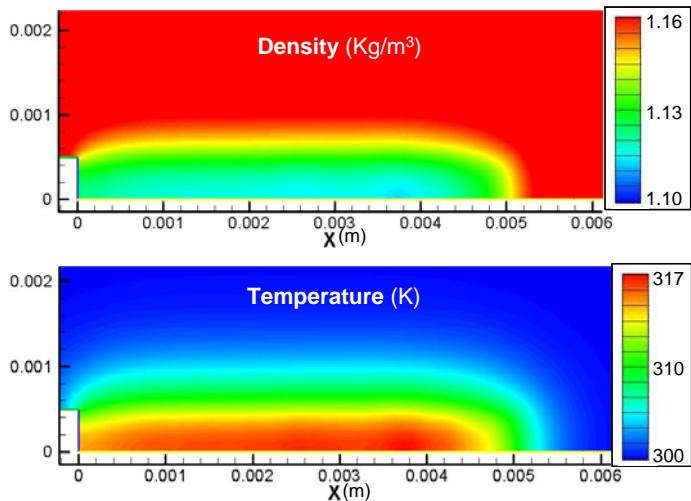

Figure 10. Density and temperature distribution contours for 10 W of heat addition at 5000Hz.

American Institute for Aeronautics and Astronautics

have reported temperature increases at the wall of about 10 degrees, therefore, the amount of power that goes directly into heating the neutrals appears to be about half of the 10W assumed in the present study. The present calculations can be treated as a worst case estimate. The density distribution is also shown in Fig. 10. It shows that the plasma actuator modifies the density over a region not much larger than the plasma. The numerically computed change is on the order of 5%. Experiments[23] show density changes of only about 2%, suggesting that, again, the heating was overestimated. It appears that density reductions observed in experiments can be accounted for solely on the basis of heat addition.

Figure 11 shows the net force generated by the plasma actuator during heat addition. Positive values represent a net drag while negative values represent a net thrust. Two force cycles are observed because each plasma bias cycle includes two heating cycles: the forward discharge and the backward discharge. Note that the thrust is only generated at the beginning of the heating cycle, when the heating zone is immediately adjacent to the edge of the exposed electrode. This occurs because the at this point, the heat induced expansion can only accelerate air downstream. At other points in the cycle, the heating accelerates air both upstream and downstream, consequently generating no net thrust. Integrating the force time history yields an average force of 0.13mN. Since typical force values generated by plasma actuators working at this power are on the order of 1.5mN, it appears that heat addition does not play a major role in the force generated by the actuator. Force generation by plasma heat addition is a function of the thickness of the exposed electrode since it is the presence of this vertical wall that allows the heat expansion to 'push'. In order to confirm this, computations were run with the exposed electrode wall removed. This is equivalent to having an exposed electrode that has zero height, or a flush mounted electrode. The heating was applied in the same manner as before and the resulting net force produced by the actuator was, as expected, zero.
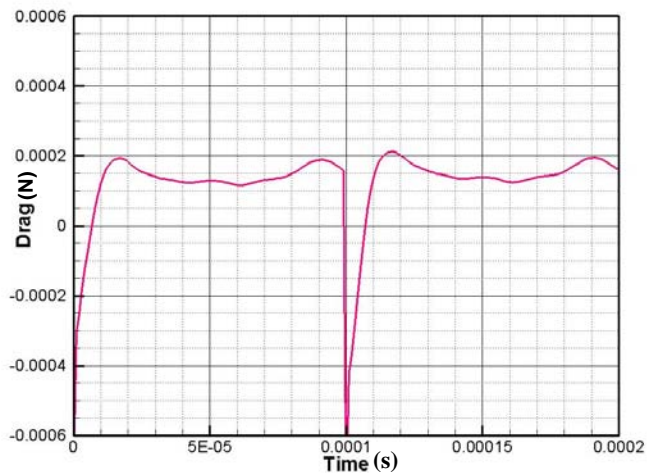
Figure 11. Net force generated by the plasma actuator during heat addition of 10W at 5000Hz. (Each plasma bias cycle has two heating cycles).

VI. Summary

Particle and fluid simulations have been carried out of a plasma actuator. PIC-DSMC simulations of a pure oxygen discharge were conducted to characterize the force vectors from a typical discharge. The results showed that the plasma actuator pulls the flow upstream during the first half of the bias cycle and pushes it downstream during the second half of the cycle. The total downstream force, however, is as much as 20 times larger than the upstream force. The force vectors and relative magnitudes were inserted into a Navier-Stokes fluid code to explore the temporal behavior of the neutrals during the discharge. Results show that the plasma actuator effect on the neutral flow is similar to a wall jet, as seen in experiments, and confirms that the effects of the force generated through particle simulations is consistent with observations. Furthermore, the upstream force during the first half of the bias cycle does not appear to be sufficiently large to reverse the direction of the flow except in a small region immediately downstream of the exposed electrode.

Particle simulations were carried out in pure nitrogen of successive discharges. The results suggested that the reason for the experimentally observed plasma expansion was due to successive streamers which charged the dielectric altering the trajectory of subsequent streamers. The altered trajectories allow the electron streamers to land farther from the exposed electrode and the plasma volume

to expand. Plasma heating of the neutrals was simulated in a fluid code using a moving heating zone, as suggested by the particle simulations and the experiments. The results show that heat addition, alone, can only account for less than 10% of the total force experimentally measured during plasma actuator operation. In addition, this force is a function of the exposed electrode thickness. Reducing the exposed electrode thickness to zero had the effect of decreasing the force to zero. The heat addition also has the effect of increasing the temperature and decreasing the neutral density in the vicinity of the plasma. The conservative estimates of heating assumed in the study were sufficient to duplicate the level of density reductions and temperature increases observed in experiments.

References

[1]Hultgren, L. S., and Ashpis, D. E., "Demonstration of Separation Delay with Glow-Discharge Plasma Actuators," AIAA Paper 2003-1025.

[2]List, J., Byerley, A. R., McLaughlin, T. E., and Van Dyken, R. D., "Using a Plasma Actuator to Control Laminar Separation on a Linear Cascade Turbine Blade," AIAA Paper 2003-1026.

[3]Roth, J. R., Sherman, D. M., and Wilkinson, S. P., "Boundary Layer Flow Control with a One Atmosphere Uniform Glow Discharge Surface Plasma," AIAA paper 98-0328.

[4]Post, M. and Corke, T., "Separation Control on High Angle of Attack Airfoil Using Plasma Actuators," *AIAA Journal*, Vol. 42, No. 11, 2004, pp. 2177.

[5]Huang, J., Corke, T. and Thomas, F., "Plasma Actuator for Separation Control of Low Pressure Turbine Blades," AIAA Paper 2003-1027.

[6]Rivir, R, White, A., Carter, C., Ganguly, B., Jacob, J., Forelines, A., and Crafton, J., "AC and Pulsed Plasma Flow Control," AIAA Paper 2004-0847.

[7]Font, G. I., "Boundary Layer Control with Atmospheric Plasma Discharges," AIAA Paper 2004-3574.

[8]Font, G. I., and W. L. Morgan, "Plasma Discharges in Atmospheric Pressure Oxygen for Boundary Layer Separation Control," AIAA Paper 2005-4632.

[9]Birdsall, C. K., and Langdon, A. B., *Plasma Physics via Computer Simulation*, Adam Hilger, Bristol, 1991, Chapter 9.

[10]Font, G. I., and Boyd, I. D., "DSMC-PIC Simulation of a Helicon Etch Reactor and Comparison with Experiments," *Process Control, Diagnostics, and Modeling in Semiconductor Manufacturing*, Electrochemical Society, 1997, pp.275.

[11]VanGilder, D. B., Font, G. I., and Boyd, I. D., "Hybrid Monte Carlo Particle-in-Cell Simulation of an Ion Thruster Plume," *Journal of Propulsion and Power*, Vol. 15, No. 4, 1999, pp.530.

[12]Li, J., and Dhali, K., "Simulation of Microdischarges in a Dielectric–barrier Discharge", *J. Appl. Phys.*, Vol. 82, No. 9, 1997, pp. 4205.

[13]Kunhardt, E. E., and Tzeng, Y., "Development of an Electron Avalanche and its Transition into Streamers," *Phys Rev. A*, Vol. 38, No. 3, 1988, pp.1410.

[14]Phelps, A. V., and Pitchford, L. C., "Anisotropic Scattering of Electrons by N_2 and its Effects on Electron Transport: Tabulations of Cross Sections and Results," JILA Data Center Report No. 26, U. of Colorado, 1985.

[15]Pitchford, L. C., and Phelps, A. V., "Comparative Calculations of Electron-swarm Properties in N_2 at Moderate E/N Values," *Phys. Rev. A*, Vol. 25, 1982, pp.540.

[16]Mitchell, J. B. A., "The Dissociative Recombination of Molecular Ions," *Physics Reports*, Vol. 186, 1990, pp.215.

[17]Ellis, H.W., Pai, R. Y., McDaniel, E. W., Manson, E. A., and Viehland, J. A., "Transport Properties of Gaseous Ions over a Wide Energy Range," *Atomic Data and Nuclear Data Tables*, Vol. 17, 1976, pp.177.

[18]Phelps, A. V., "Tabulations of Collision Cross Sections and Calculated Transport and Reaction Coefficients for Electron Collisions with O_2," JILA Data Center Report No. 28, U. of Colorado, 1985.

[19]Enloe, C. L., McLaughlin, T. E., Van Dyken, R., Kachner, K. D., Jumper, E. J., Corke, T. C., Post, M., and Haddad, O., "Mechanisms and Responses of a Single Dielectric Barrier Plasma Actuator: Geometric Effects," *AIAA Journal*, Vol. 42, No. 3, 2004, pp. 595.

[20]Enloe, C. L., McLaughlin, T. E., Van Dyken, R., Kachner, K. D., Jumper, E. J., and Corke, T. C., "Mechanisms and Responses of a Single Dielectric Barrier Plasma Actuator: Plasma Morphology", *AIAA Journal*, Vol. 42, No. 3, 2004, pp. 589.

[21]Baughn, J., Baird, C., Roney, J., Enloe, L., Font, G., and Mclaughlin, T., "Momentum Transfer for an Aerodynamic Plasma Actuator with an Imposed Boundary Layer," AIAA Paper 2006-0168.

[22]Enloe, C. L., McLaughlin, T. E., Font, G. I., and Baughn, J. W., "Parameterization of Temporal Structure in the Single Dielectric Barrier Aerodynamic Plasma Actuator", AIAA Paper 2005-0564.

[23]Enloe, C., Font, G., and Mclaughlin, T., and Baughn, J., "Frequency Effects on the Efficiency of the Aerodynamic Plasma Actuator," AIAA Paper 2006-0166.